The Preparation of Dye Sensitized Solar Cells (DSSC) using Natural dyes Extracted from Terminalia Cattappa Leaves based on Mg doped ZnO as Photoanode.

Selva Esakki E (selvaesakki7270@gmail.com)
Sri Paramakalyani College https://orcid.org/0000-0003-2287-334X
Renuga Devi L
Sri Paramakalyani College
Sarathi S
Sri Paramakalyani College
Meenakshi Sundar S
Sri Paramakalyani College

Research Article

Keywords: DSSC, Mg-ZnO, solvothermal, Terminalia cattappa, Photovoltaic

Posted Date: June 10th, 2021

DOI: https://doi.org/10.21203/rs.3.rs-589288/v1

Abstract

We report a novel type of Mg-doped ZnO nanoparticles prepared on solvothermal route nanoparticles at different concentrations (2%,4%,6%, and 8%) and used Mg-ZnO as photoanode for dye-sensitized solar cells (DSSC) fabrication. DSSC using Mg-doped ZnO as a semiconductor material and natural dyes Terminalia cattappa as sensitizer were successfully produced. The structural, optical spectra of Mg-ZnO nanopowder were studied using XRD, FESEM-EDX, TEM, SAED patterns, and UV-Visible Spectra, Fourier Transform Infrared (FT-IR). The XRD results show that the crystal size also increases by increasing the dopant concentration of the Mg-doped ZnO sample. The optical spectra show the absorption of the samples increases with the increases of concentration using the UV-Visible analysis and the bandgap energy is calculated by Tauc plot. Mg-doped ZnO nanoparticles prepared at different concentrations were used for the fabrication of DSSC. Furthermore, from the J-V graph, 8% concentration is more effective than other concentrations.

1. Introduction

One of the most important challenges in the minds of global researchers is energy storage, production, and recycling. There are many types of energy storage. One of the most important and in high demand is electricity production. Many types of solar cells have been manufactured before 1991 to generate this electricity. These include crystalline silicon solar cells, thin-film solar cells, and dye-sensitive solar cells. The third generation of solar cells is solar cell dye-sensitive solar cells. And Most researchers are heavily developing this third solar cell because this type of battery easily attracts researchers due to its low cost, high performance, and simple production[1]. There are five main materials used to make DSSC: a fluorine-topped Tin Oxide (FTO) layer, a noncrystalline wide band cap metal oxide semiconductor, working electrode, dyes, and electrolyte, and an opposite electrode [2]. FTO glass is often used for DSSC because of its low hardness, high-quality glass substrate properties such as electrical conductivity and optical transparency [3]. Next, the physical properties of ZnO nanoparticles with broadband semiconductors such as 3.37eV wide band gap energy, the higher binding energy of 60meV, good transparency, high electron mobility, and a wide variety of applications making them more widely used than TiO2 metal oxide [4]. Also, they have numerous applications in solar cells [5], optical and luminescent devices, electrical and acoustic devices, chemical sensors, catalysis, electronics[6], gas sensor devices, opto electronics, transducers, and biomedical [7-9].

The researchers adopted a number of techniques for growing ZnO NPs, including the Co-precipitation method, hydrothermal method, Sol-gel method, and Solvothermal method. Among these solvothermal methods have attracted more attention due to their slow reaction time, small particle size, and high purity of the sample [10]. In the development process of semiconductor materials, the intentional doping of an impurity in the target lattice was used as an efficient and powerful technology for adapting their electronic structures or introducing new features in traditional materials. Many research groups have examined the synthesis of ZnO NPs doped with impurities and found that a small number of dopants do not significantly change the crystal structure , but maybe slightly modified the optical, physical, and

chemical properties by forming the defect and the trap states[11]. The physical properties of the ZnO material such as resistivity, surface morphology, photocatalytic activity, and bandgap may be changed accordingly. The Mg 2+ can be easily incorporated into the ZnO array to increase the ZnO bandgap in a wide range. In recent years, Mg-doped ZnO nanostructures have been shown excellent properties for DSSC applications[12]. Thus, dopants are introduced in ZnO nanoparticles, further enhance their electrical conductivity, photon absorption and release, due to the formation of dual-stage band gap[13]and including metal ions such as Li, Al, Mn and Cr, Mg and rare earth elements has been easily doped into the ZnO lattice by using this method. Each of these metal dopants possesses a unique ability to elevate the properties of ZnO nanoparticles, it can be also seen from the literature that metal doping into ZnO has an important effect to improve their photovoltaic parameters of ZnO based DSSCs. However, the Mg-doped ZnO nanoparticles are synthesized in the present work as they exhibit promising photovoltaic activity for pollutants with respect to pure ZnO. On the other hand, the performance of solar cells depends on the sensitivity. Natural dyes have several advantages compared to metal complexes (ruthenium-based complexes) because of easy extraction with the lowest chemical procedures, large absorption coefficients, low cost, non-toxic, environmentally friendly, and wide availability[14]. Moreover, synthetic dyes have been full of problems, such as complicated and low harvest. Accordingly, several dyes extracted from natural pigments including anthocyanins, carotenoids, and chlorophylls have been used as sensitizers in DSSC. The advantage of geoxanthine is that it allows the binding of carbonyl and hydroxyl groups of xanthophylls on the surface of a metal oxide nanoparticle. This helps for anchoring the dye on the surface of ZnO film and additionally provides easy electron transfer from the zeaxanthin molecule to the conduction band of ZnO. Although dyes have a good photoelectric conversion efficiency, their long-term use in DSSCs is not sustainable because of the limited sources of ruthenium, and the high cost associated with the production of ruthenium complex dyes [15]. Next, an electrolyte is the fourth most important component for dye-sensitized solar cells. The properties of this electrolyte such as conversion efficiency and stability have a major impact on the efficiency of solar cells. Commonly used substances in electrolytes for dye-sensitized solar cells are KI and LI, acetonitrile. These precursors are used to reduce the recombination of electrons in the conduction band of the semiconductor and to accept electrons in the electrolyte through the semiconductor surface. Then, the photovoltaic filler factor and the conversion efficiency increase to a higher level [16]. Finally, the counter electrode is the fifth important component of solar cells. The carbon is coated on the opposite electrode. Graphite and platinum are often used for this purpose. The main benefit of carbon is that platinum is commonly used as a counter electrode to react with the triiodide ions formed in the electrolyte by reducing the iodide ions. The platinum counter electrode gives higher performance than other carbon. However, due to its high cost, instability in redox electrolyte, high-temperature sintering, and lack of resources, the researchers did not attract attention. But many carbon products used as counter electrodes show lower catalytic activity compared to pt. This can be offset by increasing the active area of the catalyst layer using a porous structure [17].

In this present work, synthesize and characterization of pure and Mg-doped ZnO nanoparticles with various concentrations of Mg contents are prepared by using the solvothermal microwave method. The

structural, optical, thermal, and electrical properties of Mg-doped ZnO are explored. Furthermore, the production of dye-sensitive solar cells using natural dyes based on Mg-doped ZnO at different concentrations (2%, 4%, 6%, and 8%) using the Terminalia cattappa is being studied. In addition, the study illustrates a correlation between the morphology of the pure and Mg-doped ZnO samples and the J-V to clarify the reason for the increase in energy conversion efficiency values

2. Experimental

2.1. Preparation of Mg doped ZnO nanoparticle with different concentration:

Analytical grade precursor materials like Zinc acetate dihydrate, Urea (H_2NCONH_2) were accustomed to synthesis ZnO nanoparticles by solvothermal technique. Ethylene glycol [$CH_2OH.CH_2OH$] is used as a good solvent to dissolve all substances. Four samples for this study were compiled at different concentrations of 2%, 4%, 6%, and 8%. During this method, Zinc acetate dihydrate and urea within the 1:3 ratios were mixed and dissolved in 50 ml of ethylene glycol and thus the mixture was stirred well for 1hour using a magnetic stirrer. The mixed solution is placed in a domestic microwave oven at a temperature of 80 °C. Microwave radiation is applied until the solvent is completely dissolved. Furthermore, the irradiated sample is cooled to room temperature and washed at least four times in double-distilled water and acetone to remove organic contaminants from the samples. The synthesized nanoparticles are filtered, dried at 60 ° C for half an hour, and placed in a muffle furnace at 500 ° C for 2 hours to enhance the crystallization of the samples. [18,19]

2.2 Fabrication of DSSC:

The conductive glass is a fluorine-topped tin oxide (FTO) with a base resistance of 7 ohms / square dimensions L × 25 mm W × 25 mm D × 2.2 mm sheet resistance. The glass substrates were cleaned with a soap solution using an ultrasonic bath for 10 minutes, washed with distilled water and ethanol, and then dried. The ZnO paste was prepared by adding 3.5 gm of ZnO nanopowder, 1ml acetic acid, and 4ml of ethanol, 5ml of distilled water, and 2 drops of Triton X-100. Then, using a magnetic stirrer, grind the mixture for half an hour until a homogeneous paste appears. The ZnO nanoparticle films were prepared by the doctor blade technique. The edges of a conducting glass (Technistro, Maharashtra) were covered with adhesive tapes on the frame. ZnO paste rolls on an FTO glass plate using a glass rod. Films with different thicknesses were fabricated by adjusting the concentration of the paste [20]. And the area of the coated glass was 0.5 cm2. The ZnO-coated FTO glass plate is then dried on a 60 ° C hot plate for 20 minutes. Finally, the samples were sintered at 450°C for 30 minutes. They were cooled down up to 70°C. The natural dye was extracted and purified following the procedure reported in the literature [21]. Almond leaves (Terminalia kattappa) are distilled, washed in water, and are then soaked in absolute ethanol at room temperature in the dark for a day to extract the dye. The solids were filtered out, and the filtrates were concentrated at 60°C for use as sensitizers. The cherry-red solution appeared within an hour. The working electrode is soaked in almond dye solution for one day. Carbon was coated on the FTO glass substrate as a counter electrode using a graphite pencil. The fabricated

The working electrode and the opposite electrode are both connected together. An electrolyte solution containing 0.8 g KI, 10 ml acetonitrile, 0.127 g I2, etc. Was prepared, and the solution was stirred for 30 min and then stored in a sealed bottle. Two drops of electrolyte solution were injected between the two electrodes and the cell was immediately tested under a J-V measurement.

2.3 Characterization and measurements:

The Mg-doped ZnO nanoparticle with different concentration of (2%,4%,6%, and 8%) nanoparticles was characterized by X-ray diffractometer XPERT-PRO, Surface morphology of the prepared films were studied using a scanning electron microscope (FE-SEM) (EVO 18 SEM), and the elemental composition of samples was analyzed using energy dispersive x-ray spectroscopy EDAX (QUANTA – FEG 250). TEM and SAED patterns were recorded using JEOL JEM-2100 Electron Microscope. The Fourier Transmission Infra-Red (FTIR) spectra were recorded using NICOLETIS5 –KBR windows with AR diamond crystal plate to analyze the functional groups of the natural dyes. The UV-Visible absorption was recorded using (HITACHI UH 5300) and TGA curves were recorded using a TA instrument model- SDT-Q600. Electrochemical impedance spectroscopy measurements were recorded using the electrochemical workstation at room temperature at the frequency of 100 to 106 Hz. A solar simulator was used to simulate sunlight under one sun AM 1.5G (100 mW/cm^2) illumination provided by a 300 W xenon lamp was employed for J-V measurements

3. Results And Discussion

3.1 Structural analysis

Fig.1 shows the XRD pattern of pure ZnO and Mg-doped ZnO nanoparticles of different concentrations (2, 4, 6, and 8%) of Mg. The XRD method of pure and Mg-doped ZnO nanoparticles shows the comparison with JCPDS data card number 80-0075, with the triplet sharpest peaks 31.83, 34.57, and 36.37 dominating at 2θ. These 2θ values are associated with the hexagonal wurtzite structure with corresponding planes of (100), (002), and (101). Moreover, the triplet peak intensities (100), (002), and (101) of pure ZnO are suppressed without any change in its phase due to the addition of higher wt% of Mg. This is supported by the emergence of additional peaks in the directions of (102), (110), (103), (200), (112), (201), and (202) indicating the formation of the hexagonal wurtzite structure. But there is no various impurity peak as determined within the XRD patterns showing the single-phase formation. It was found that the addition of Mg did not have an effect on the structure of ZnO [22]. Average crystallite size D for ZnO nanoparticle was calculated using the Debye-Scherrer formula which is given in Eq (1).

$$\mathbf{D} = \frac{K\lambda}{\beta cos\theta} \quad \ldots\ldots\ldots\ldots(1)$$

where K=0.89 is the Debye Scherrer constant, β is the full width at half maximum (radians), λ is the wavelength of the X-ray sources (0.1540nm), and θ is the peak positions (radians). it was observed that the average crystallite size calculated across 11nm, 13nm, 18 nm, and 24nm for the samples obtained at Mg doped ZnO. The Calculation shows that the acs (particle size) increases from 11 to 24 nm with an increase in the concentration of Mg doping and the calculation also depicts that the intensity of the XRD peak decreases as the Mg doping concentration increases [23]. The reason behind enhancing crystalline size due to that the incorporation of magnesium dopants reduces the intensity of (100), (002), and (101) planes by 8% [24]. It is observed that the peaks shift towards lower angles and the intensities of the peaks decrease with higher Mg doping in ZnO, indicating that the dopant Mg2+ ions are substituted in the Zn2+ ions. It can be noted that the average crystallite size of the ZnO nanoparticle increases from 11 to 18 nm with an increase of Mg content from 0% to 8%.[25].

where K=0.89 is the Debye Scherrer constant, β is the full width at half maximum (radians), λ is the wavelength of the X-ray sources (0.1540nm), and θ is the peak positions (radians). it was observed that the average crystallite size calculated across 11nm, 13nm, 18 nm, and 24nm for the samples obtained at Mg doped ZnO. The Calculation shows that the acs (particle size) increases from 11 to 24 nm with an increase in the concentration of Mg doping and the calculation also depicts that the intensity of the XRD peak decreases as the Mg doping concentration increases [23]. The reason behind enhancing crystalline size due to that the incorporation of magnesium dopants reduces the intensity of (100), (002), and (101) planes by 8% [24]. It is observed that the peaks shift towards lower angles and the intensities of the peaks decrease with higher Mg doping in ZnO, indicating that the dopant Mg2+ ions are substituted in the Zn2+ ions. It can be noted that the average crystallite size of the ZnO nanoparticle increases from 11 to 18 nm with an increase of Mg content from 0% to 8%.[25].

3.3.EDAX analysis

The EDAX spectrum of solvothermal synthesized Mg-doped ZnO nanoparticles with different Mg concentrations of (2,4, 6, and 8 wt%) is shown in Fig 3. The results confirm the presence of expected elements such as Zn, Mg, and O. In addition, all the samples have good stoichiometric properties. which is indicates the uniform distribution of Mg inside the ZnO lattice. The table shows the atomic percentage of Mg-doped ZnO nanoparticles. Obviously, the atomic % of Mg was found to increase and the corresponding Zn reduced considerably for 6 wt% of Mg. This indicates the strong incorporation of Mg in the host ZnO, which is in good accordance with our FE-SEM results. Moreover, the oxygen content is also unstable after incorporating the Mg.

Table 1: Elemental analysis of Mg doped ZnO at various concentrations

wt% of Mg	Atomic %		
	Zn	O	Mg
2	58.80	40.76	0.44
4	44.21	54.44	1.34
6	40.08	56.82	3.10
8	52.09	47.91	0.00

3.4 TEM analysis of Mg doped ZnO nanparrticle:

The TEM images of Mg-doped ZnO nanoparticles are shown in Fig. The Mg-doped ZnO sample exhibits a spherical-like morphology however, the encasing of ZnO with Mg is random. The inset in Fig. (a) clearly shows the ZnO encased Mg nano spherical in shape. SAED patterns of the sample is given in Fig (b). The SAED pattern of Mg coated ZnO nano spherical shows a continuous diffraction ring with a bright spot indicating the crystalline nature. This analysis confirms the single phased ZnO compound and such results are consistent with XRD planes.

3.3 Optical studies

The absorption spectra of natural dyes extracted from Terminalia cattappa were analyzed using the UV-Visible Spectrophotometer and shown in Figure 5. The leaves of Terminalia cattappa show the UV-visible absorption spectrum of the dye solution extracted from ethanol as a solvent. It was found that absorption peaks detected the presence of zeaxanthin in the range of 304nm and 364nm. The absorption edge can be identified clearly about wavelength 304 nm which is the optical transition occurs. The bandgap values of the extracted natural dyes of almond leaves were found to be 2.32 eV using the Origin showed in figure 6.

The UV- Visible absorption spectra of Mg-doped ZnO NPs as a function of wavelength for the range of 300 to 800 nm are shown in figure 7. From the figure, it is observed that the absorption peak increases with the concentration of Mg increases and which indicates that Mg2+ ions are incorporated into the ZnO lattice. The absorption ranges for doping concentrations of 2%, 4%, 6%, and 8% are 244 nm, 248nm, 372 nm, and 378 nm, respectively. The inherent reason for increases in absorbance may be due to various factors like particle size, oxygen deficiency, and defects in grain structure [27].

The bandgap energy of the Mg-doped nanoparticles measured using the Tauc plot. It is noted that the samples exhibit concentration dependence of bandgap. The bandgap energy decreases from 3.36eV to 1.65eV. Therefore the bandgap energy is decreased by the increases in the absorbance and decreases in bandgap energy confirm the presence of Mg2+ inside the Zn2+ site of the ZnO lattice.[28].

3.4 FTIR analysis

The chemical structure of the extracted natural dyes was studied using FTIR. The natural dyes want to own specific functional groups in order to effectively absorb the metal-oxide materials [29]. Fig 9 shows that the zeaxanthin dye extracted from almonds shows broad and strong peaks at 3297.87 cm-1 and due to the presence of hydroxyl group in stretching vibration mode. The peaks at 1081.36 cm-1 and 1032.47 cm-1 represented the stretching vibrations of the C-O-C ester. C=O stretching vibration shows a peak at 1734.37 cm-1. As observed from the functional groups of zeaxanthin dye extracted from the almond leaves. And bending of carbonate is observed at 862.58 cm-1. The functional groups confirm the presence of zeaxanthin in the almond dye [30]. All metal oxide nanoparticles can be found below 500 cm-1.

3.5 Electrochemical impedance spectral (EIS) studies:

The internal resistance and charge transfer kinetics Mg-doped ZnO photoanodes in standard solar irradiation AM 1.5 (100mW/cm-2) with 0.5 V applied bias voltage at room temperature by measuring the Electrochemical impedance spectroscopy (EIS). X and Y axis real and imaginary parts of the impedance respectively. Figure 11 displays the obtained Nyquist plots of DSSCs fabricated in the frequency range of 100 to 106 Hz. The Nyquist plots show the impedance of the system has a semicircle. It depends on the applied potential. The efficiency decreases by increasing the radius of the semicircle.y. Z VIEW software was used for impedance spectra analysis based on an equivalent circuit consisting of a series of parallel RC circuits. The electron transfer resistance (Rpt) at counter electrode/electrolyte in the high-frequency region, charge transfer resistance (Rct) at the photoelectrode/electrolyte interface appear in the middle frequency region, the diffusion impedance (Zd) of the redox couple in the electrolyte, and the chemical capacitance (Cμ) were directly obtained from the fit. And the Mg-doped ZnO at 8%, showed a smaller impedance compared to ZnO at 2%, the DSSCs based on 2% showed higher impedance to recombination than the other concentrations. The smaller radius indicated faster charge recombination appeared in the cell.

Bode plot:

In Figure 12 shows plots of phase angle changes with frequency for ZnO nanoparticles. Bode's plots are given the electron lifetime in the ZnO conduction band. The electron lifetime has been appraised using the formula for Mg-ZnO

$\tau CB = 1/2\pi f$ …….(2)

where τCB - a lifetime of an electron in the CB of ZnO, f- middle of frequency peak. Lifetime values are 0.46 and 0.54 with concentrations of Mg-doped ZnO at 2% and 8%, respectively. Bode plots showed the frequency of maximum phase angle increased with the phase angle decreasing to semiconductor value of 45.71° and 52.23° for Mg-doped ZnO at a concentration of 2% and 8% nanoparticles

3.6 Thermo gravimetric analysis (TG)

The thermal properties of the precursor were determined by thermogravimetric analysis. In Figure 11, the TG curve of the synthesized Mg-doped ZnO-NPs shows a gradual weight loss from 10- 50 °C-(19.50 mg) due to the evaporation of water, alkaline groups, and organic compounds present in the nanoparticles and continuous weight loss occurred between 22.4°C(16.97 mg),270.4 °C(11.69mg)and 412 °C (10.01mg). Later, a plateau region is formed at a temperature above 450°C .which confirmed the formation of highly stable ZnO-NPs. In figure 8 b the TG curve of the synthesized Mg-doped ZnO at a concentration of 4%, the function of temperature in the range from 20 to 500°C. A gradual weight loss is 56.3°C (4.37 mg) due to the evaporation of water, alkaline groups, and organic compounds present in the nanoparticles, and continuous weight loss occurred between 212.2 °C (2.975 mg) and 256 °C (-0.119mg). Later, a plateau region is formed at a temperature above 400°C which confirmed the formation of highly stable ZnO-NPs. This is confirmed by the weight loss observed in the temperature region 400–600°C in the TGA curve[32] When the thermogravimetric analysis is performed, a particle is deformed by the use of heat, which causes bonds within the molecules to be broken. The weight of the sample goes down slowly as the reaction begins, then decreases rapidly over a comparatively narrow temperature range, and finally levels off as the reactants become spent. The shape of the TGA curve is primarily determined by kinetic parameters [33].

3.7.J-V characteristic of fabricated DSSC:

Figure 12 shows the J-V curve of the DSSC-produced Mg-doped ZnO sample, placed under AM 1.5G sunlight at 100 MW / cm2. It has been noted that the short circuit current density varies from 0.79 to 1.09 mA / cm2. For 2% of Mg-doped ZnO-based DSSC, the efficiency is obtained at 0.39%. After 4% of Mg doping ZnO, the efficiency was reached 0.43%. it can be attributed to the increase of Jsc values. And also adding 45% Mg doping ZnO-based DSSC, shows the efficiency was 0.47%. Then the increase of 8% Mg doping ZnO-based DSSC, exhibit the best overall efficiency is 0.53%. it can be seen in figure 11, the increase of short current density and fill factor with increases of solar cell efficiency. It can be seen that the JSC value of DSSC has increased by increasing the Mg-doping level. This may be due to an increase in Jsc values, image changes, and a decrease in intensity in the XRD data [34,35]. That is seen in FE-SEM analysis, 2% and 4% of Mg-doped ZnO samples have large surfaces. And also adding 6% and 8 % of Mg-doped ZnO samples have a cluster of hexagons molecules. Therefore the bandgap values of Mg-doped ZnO of our samples increase with increases in Mg doping level. And this increase in the bandgap value corresponds to a rise in the efficiency of the fabricated DSSCs[36]. It absorbs the high energy of photons on the surfaces. The Mg concentration could cause more efficient electron transport that might also increase the Jsc values.

The light energy to electrical energy conversion efficiency η is calculated from the photoelectron chemical parameters using the formula.

$$\eta(\%) = \frac{(FFxI_{sc}xV_{oc})}{P_{in}} x100 \text{.....(3)}$$

where Pin denotes the energy of the incident photon.

$$FF = \frac{(I_{max} x V_{max})}{(I_{sc} x V_{oc})} x100 \ldots\ldots\ldots\ldots\ldots\ldots(4)$$

where Imax and V max denote the maximum output value of current and voltage respectively, and Isc and Voc denote the short circuit current and open-circuit voltage respectively.Through the result obtained is better than the reports for DSSC fabricated with ZnO photoanodes [27-29], the efficiency observed in this study could be due to the synthesis of dopant and concentration variation.

Table: 2 .Photovoltaic performance of Dye Sensitized Solar cell

Dyes	Semiconductor	V_{oc} (V)	J_{sc} (mA/cm^2)	FF	Efficiency	Referance
N719	Mg-ZnO	(mV)				37
	0%	251	2.38	0.34	0.21	
	0.4%	390	3.44	0.34	0.47	
	0.6%	488	3.30	0.35	0.57	
	1%	575	3.00	0.42	0.71	
N719	Mg-ZnO					36
	0%	0.38	0.111	0.12	0.0054	
	2%	0.45	0.235	0.46	0.05	
	4%	0.48	0.368	0.44	0.08	
	6%	0.39	0.034	0.33	0.00047	
N719	Mg-ZnO					38
	0%	0.56	6.08	50.1	1.72	
	2%	0.60	11.18	62.5	4.19	
Tamarinila cattappa	Mg-ZnO					
	2%	0.99	0.79	0.50	0.39	
	4%	0.99	0.87	0.53	0.43	
	6%	0.99	0.95	0.57	0.47	
	8%	0.99	1.09	0.60	0.53	

Conclusion

Mg-doped ZnO nanoparticles have been successfully synthesized via an easy method of solvothermal microwave irradiation techniques. The structural, morphological, optical, electrical, and thermal properties of the synthesized samples were characterized by XRD, FRSEM, EDAX, TEM, FTIR, UV-Visible, and EIS, TGA analysis. The average crystallite size of Mg-doped ZnO nanoparticle with different concentrations is found to be 11nm to 24 nm with hexagonal wurtzite structure as observed from XRD results. FESEM images exhibit the formation of hexagonal plates in the prepared samples. The EDAX analysis has confirmed the presence of Mg. Zn, O elements.TEM morphology shows the improvement of crystal-shaped ZnO nanoparticles with a regular arrangement of lattice fringes in the SAED patterns. The FTIR analysis demonstrates the confirmation of metal oxide nanoparticles. And UV-Visible spectra determined the band gap value using the Tauc plot method. And EIS spectra show that the semicircle of radius decreases with the increase of conductivity. Then the thermal studies exhibit a weight loss in the given sample. DSSC was fabricated using the prepared Mg-doped ZnO nanostructures at different concentrations and Terminalia cattappa dye, the efficiency observed. At concentration, 8% showed 0.53% efficiency and is comparatively better than the concentration of 2% due to the bandgap value decreased.

Declarations

Complicit Interest

The authors declare that they have no conflict of interest.

Acknowledgement:

The authors are very much thankful to Sri Paramakalyani College, Alwarkurichi, Sri Ramakrishna Mission Vidhyalaya Arts and Science College, Coimbatore. And University of Karpagam for providing instrumental facilities.

References

1. B. O'Regan, M. Grätzel, A low-cost, high-efficiency solar cell based on dye sensitized colloidal TiO2 films, Nature 353 (1991) 737–739.

2. Sofyan A. Taya, Kamal S. Elrefi, Taher M. El-Agez, Monzir S. Abdel-Latif, dye sensitized solar cells using fresh and dried natural dyes, Turk. J. Phys. 39 (2015) 24e30.

3. Aakash Umesh Bhanushali, Sachin Yadav, R. Pratibha Nalini, Spinach and beetroot extracts as sensitizers for ZnO based DSSC, Int. J. Eng. Sci. Manag. Res. 2 (5) (2015) 37e42.

4.Ravichandran C, Kumar J, Srinivasan G, Lennon Craig, Sivananthan S, J Mater Sci. Mater Electron 2015;26;5489-94.

5. Vanaja, Aravapalli, M. Suresh, and Jaison Jeevanandam. "Facile Magnesium Doped Zinc Oxide Nanoparticle Fabrication and Characterization for Biological Benefits." *International Journal of Nanoscience and Nanotechnology*15.4 (2019): 277-286.

6. Wang, Zhong Lin. "Zinc oxide nanostructures: growth, properties and applications." *Journal of physics: condensed matter*16.25 (2004): R829.

7. Zare, Elham, et al. "Simple biosynthesis of zinc oxide nanoparticles using nature's source, and it's in vitro bio-activity." *Journal of Molecular Structure*1146 (2017): 96-103.

8. Cheng, Yuanhang, et al. "Decomposition of organometal halide perovskite films on zinc oxide nanoparticles." *ACS applied materials & interfaces*7.36 (2015): 19986-19993.

9. Dizaj, Solmaz Maleki, et al. "Antimicrobial activity of the metals and metal oxide nanoparticles." *Materials Science and Engineering: C*44 (2014): 278-284.

10. Guruvammal, D., S. Selvaraj, and S. Meenakshi Sundar. "Effect of Ni-doping on the structural, optical and magnetic properties of ZnO nanoparticles by solvothermal method." *Journal of Alloys and Compounds* 682 (2016): 850-855.

11 Liu, Siyi, et al. "Defect-related optical properties of Mg-doped ZnO nanoparticles synthesized via low temperature hydrothermal method." *Journal of Alloys and Compounds* 858 (2021): 157654.

12. Etacheri, Vinodkumar, Roshith Roshan, and Vishwanathan Kumar. "Mg-doped ZnO nanoparticles for efficient sunlight-driven photocatalysis." *ACS applied materials & interfaces*4.5 (2012): 2717-2725.

13. Simeonidis, Konstantinos, et al. "Inorganic engineered nanoparticles in drinking water treatment: a critical review." *Environmental Science: Water Research & Technology* 2.1 (2016): 43-70.

14. Pratiwi DD, Nurosyid F, Supriyanto A, Suryana R. Performance improvement of dye-sensitized solar cells (DSSC) by using dyes mixture from chlorophyll and anthocyanin. InJournal of Physics: Conference Series 2017 Nov 1 (Vol. 909, No. 1, p. 012025). IOP Publishing.

15. Chinaka CN, Ezealisiji KM, Akpofure RE. Phyto-chemical Characterization of the Leaf extracts of Terminalia catappa L.(Combretaceae) Using Ultra violet-Visible, Fourier transform infrared and Gas chromatography-Mass Spectroscopic techniques. Journal of Pharmacognosy and Phytochemistry. 2018;7(1):2017-23.

16.Kong FT, Dai SY, Wang KJ. Review of recent progress in dye-sensitized solar cells. Advances in OptoElectronics. 2007;2007.

17.Kim SS, Nah YC, Noh YY, Jo J, Kim DY. Electrodeposited Pt for cost-efficient and flexible dye-sensitized solar cells. Electrochimica Acta. 2006 May 5;51(18):3814-9.

18. Guruvammal D, Selvaraj S, Sundar SM. Structural, optical and magnetic properties of Co doped ZnO DMS nanoparticles by microwave irradiation method. Journal of Magnetism and Magnetic Materials. 2018 Apr 15; 452:335-42.

19.Varadhaseshan R, Sundar SM. Existence of ferromagnetism and structural characterization of nickel doped ZnO nanocrystals. Applied surface science. 12012 Jul 1; 258(18):7161-5.

20. Selva Esakki Meenakshi Sundar , Fabrication Of Natural Dye Sensitized Solar Cell Using Sunflower, Indian Almond Fruit And Pongame Oil Tree Leaf Extracts With Tio2 Photoanode International journal of scientific and tecnology research . volume 9, issue 3, march 2020

21..El-Agez, T. M., El Tayyan, A. A., Al-Kahlout, A., Taya, S. A., & Abdel-Latif, M. S. (2012). Dye-sensitized solar cells based on ZnO films and natural dyes. *International Journal of Materials and Chemistry*, *2*(3), 105-110.

22. Synthesis and characterization of Mg-doped ZnO hollow spheres. *Journal of Nanoparticle Research*, *13*(5), 2205-2212.

23. Johan, Mohd Rafie Bin, et al. "Influence of Mg Doping on ZnO Nanoparticles for Enhanced Photocatalytic Evaluation and Antibacterial Analysis." (2018).

24. Vanaja A, Suresh M, Jeevanandam J. Facile Magnesium Doped Zinc Oxide Nanoparticle Fabrication and Characterization for Biological Benefits. International Journal of Nanoscience and Nanotechnology. 2019 Nov 1;15(4):277-86.

25. Rouchdi, M., et al. "Synthesis and characteristics of Mg doped ZnO thin films: Experimental and ab-initio study." *Results in physics* 7 (2017): 620-627.

26. Nursyahadah MZ, Nurul SS, Azlan Z, Kumar MT. Effect of magnesium doping on structural and optical properties of ZnO nanoparticles synthesized by mechanochemical processing. In AIP Conference Proceedings 2011 Mar 30 (Vol. 1328, No. 1, pp. 211-213). American Institute of Physics.

27. Guruvammal D, Selvaraj S, Sundar SM. Structural, optical and magnetic properties of Co doped ZnO DMS nanoparticles by microwave irradiation method. Journal of Magnetism and Magnetic Materials. 2018 Apr 15; 452:335-42

28. Johan, Mohd Rafie Bin, et al. "Influence of Mg Doping on ZnO Nanoparticles for Enhanced Photocatalytic Evaluation and Antibacterial Analysis." (2018).

29. H.Chang , M.J.Kao, T.L.Chen,C.Cho and X.R.Lai ‘characterization of natural dye extracted from wormwood and puple cabbage for dye-sensitized solar cells”, International journal of Photoenergy ,Vol.2013,Aticle ID 159502, 8pages,2013

30. Ganta D, Jara J, Villanueva R. Dye-sensitized solar cells using aloe vera and cladode of cactus extracts as natural sensitizers. Chemical physics letters. 2017 Jul 1;679:97-101.

31. Shan C, Yang H, Song J, Han D, Ivaska A, et al. (2009) Direct electrochemistry of glucose oxidase and biosensing for glucose based on graphene. Anal Chem 81: 2378-2382.

32. Rokhum, S. L., Biswas, A., Changmai, B., Chhangte, V., Lalfakzuala, R., & Nath, S. (2020). Biosynthesis of Triangular-Shape ZnO Nanoparticles Using Tecoma Stans and Its Antimicrobial Activity

33. El-Kader, F. A., Hakeem, N. A., Elashmawi, I. S., & Ismail, A. M. (2013). Structural, optical and thermal characterization of ZnO nanoparticles doped in PEO/PVA blend films. *Aust. J. Basic Appl. Sci*, *7*(10), 608-619

34. Ye, Ning, et al. "Improvement of the performance of dye-sensitized solar cells using Sn-doped ZnO nanoparticles." *Journal of Power Sources* 195.17 (2010): 5806-5809.

35. Nayeri, F. Dehghan, E. Asl Soleimani, and F. Salehi. "Synthesis and characterization of ZnO nanowires grown on different seed layers: the application for dye-sensitized solar cells." *Renewable Energy* 60 (2013): 246-255.

36. Polat, Ismail, et al. "Role of Mg doping in the structural, optical, and electrical characteristics of ZnO-based DSSCs." *Turkish Journal of Physics* 41.2 (2017): 160-170.

37. Duan Z, Du Pasquier A, Lu Y, Xu Y, Garfunkel E. Effects of Mg composition on open circuit voltage of Cu2O–MgxZn1− xO heterojunction solar cells. Solar energy materials and solar cells. 2012 Jan 1;96:292-7.

38. Guo X, Dong H, Niu G, Qiu Y, Wang L. Mg doping in nanosheet-based spherical structured ZnO photoanode for quasi-solid dye-sensitized solar cells. RSC advances. 2014;4(41):21294-300.

Figures

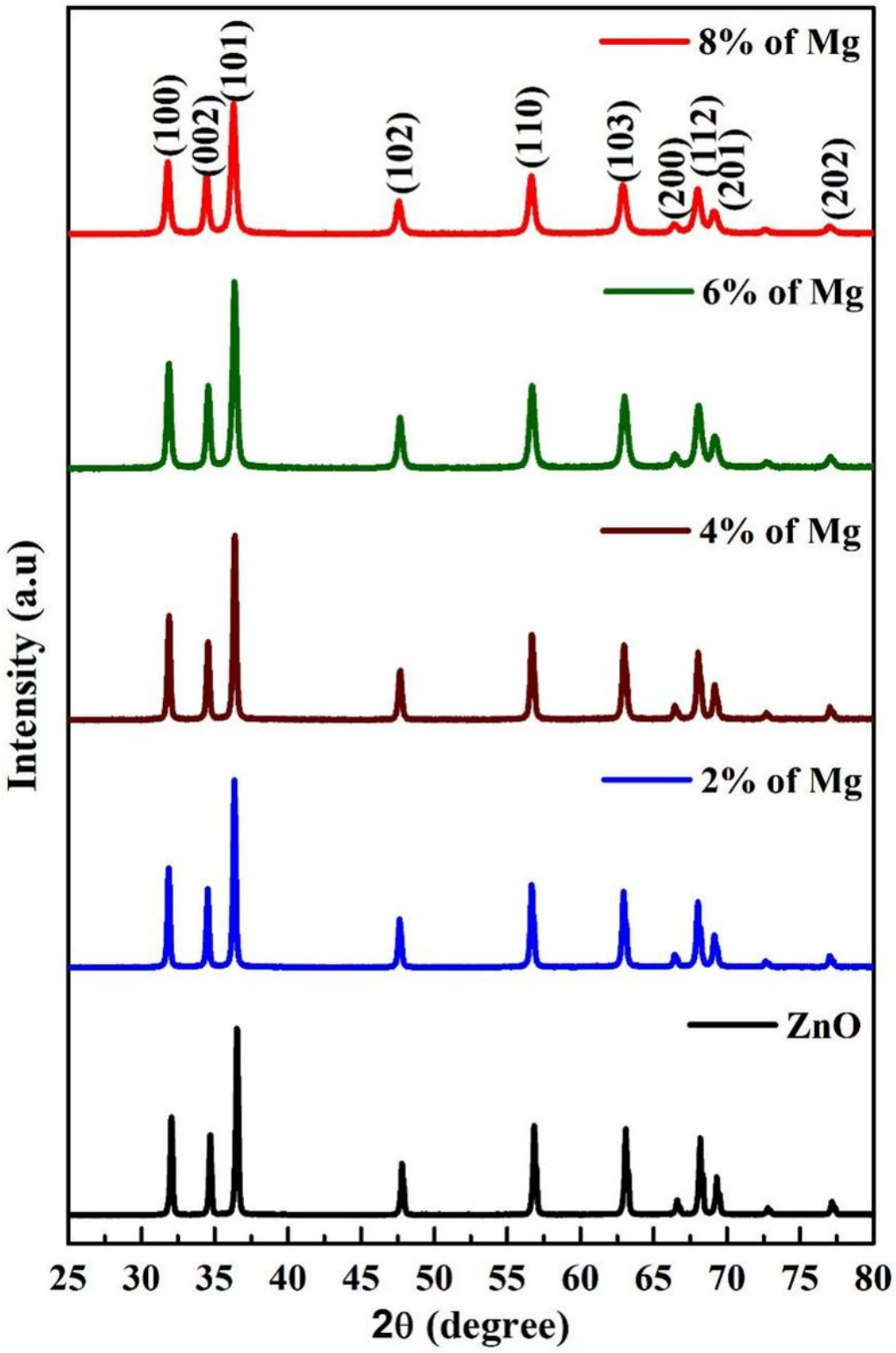

Figure 1

XRD patterns of pure ZnO with various concentration of Mg dopants

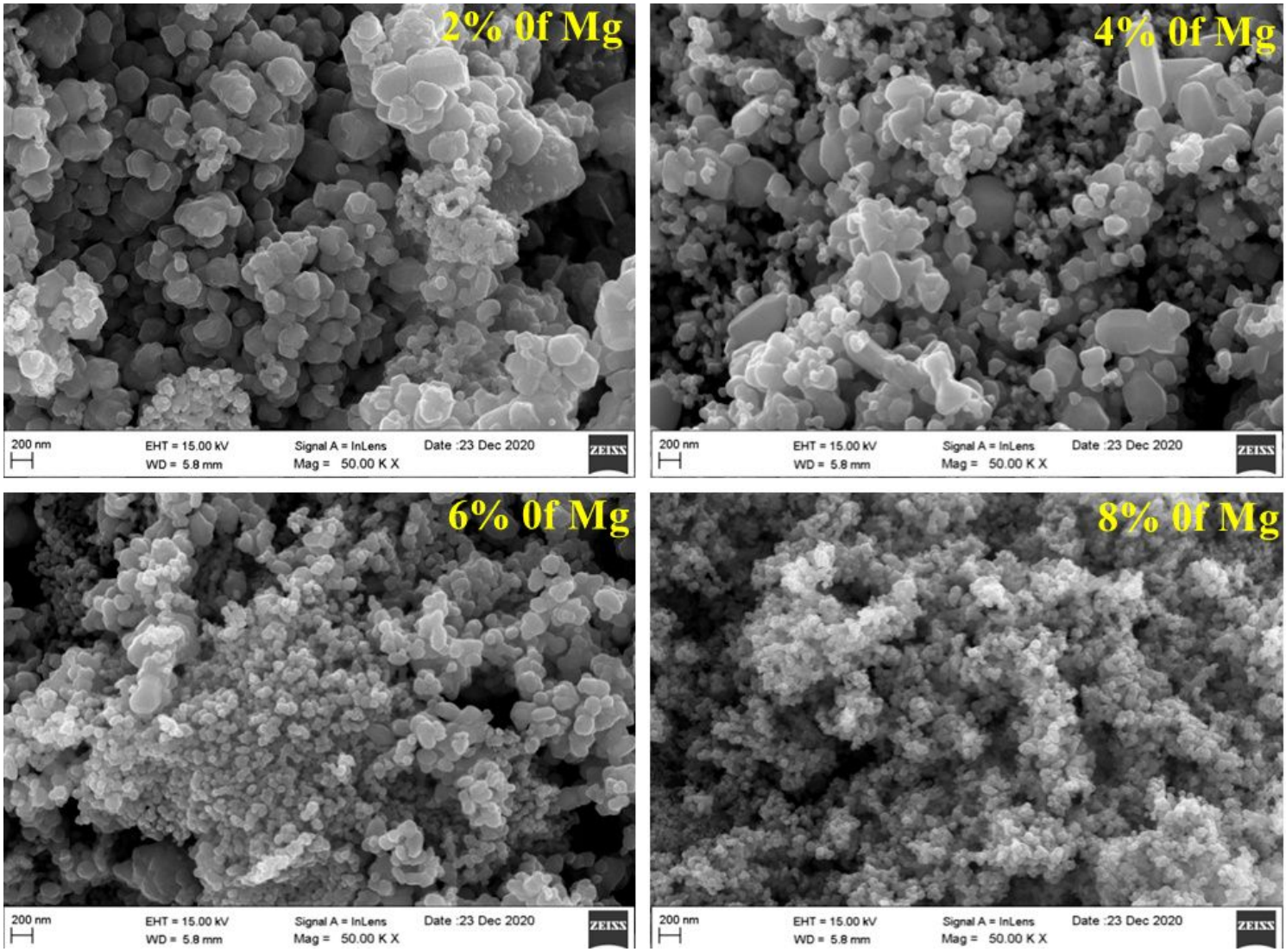

Figure 2

FESEM images of Mg doped ZnO nanoparticles.

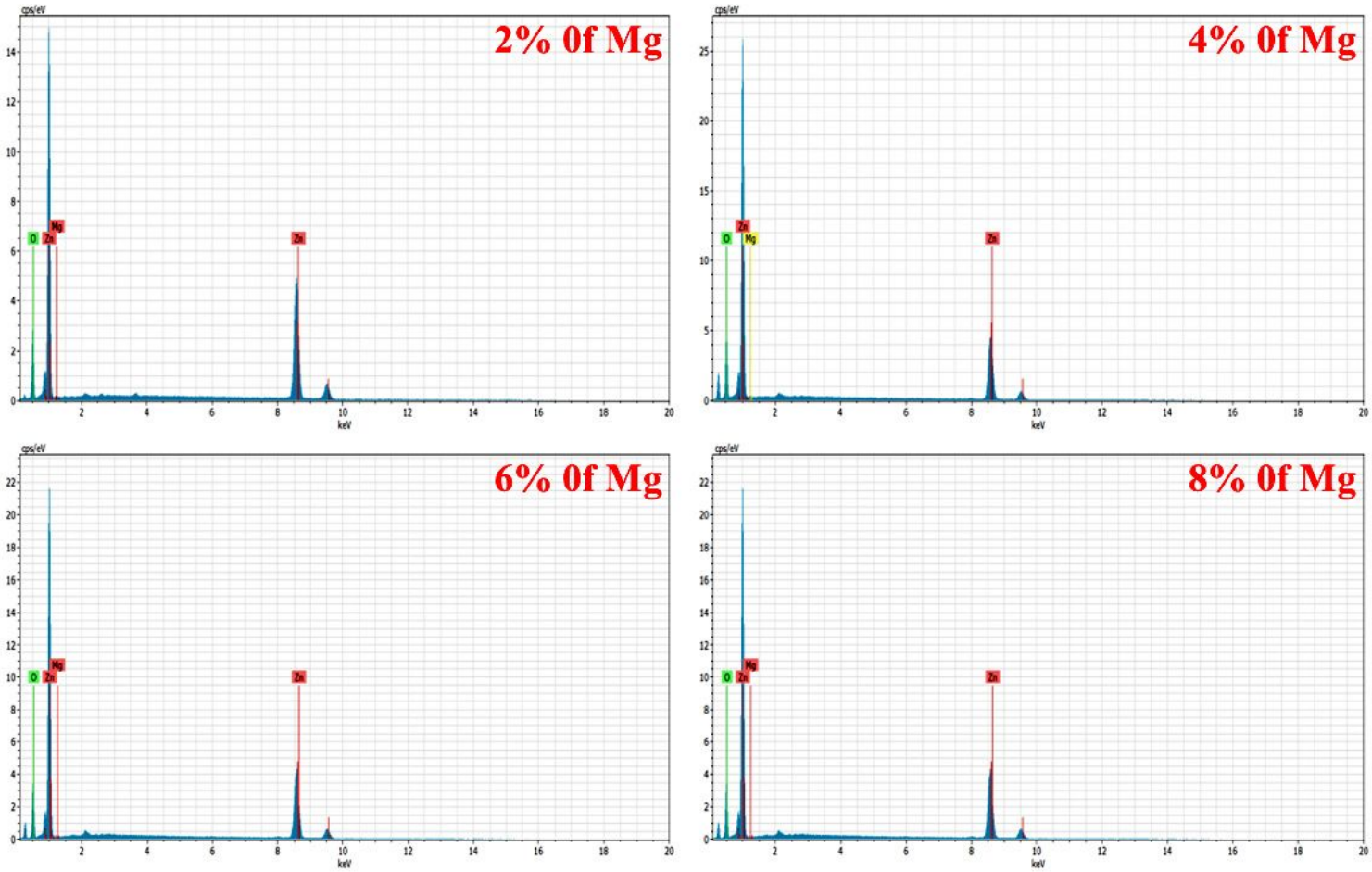

Figure 3

EDAX- elemental composition spectra of 2%,4%,6% and 8% fo Mg doped ZnO samples.

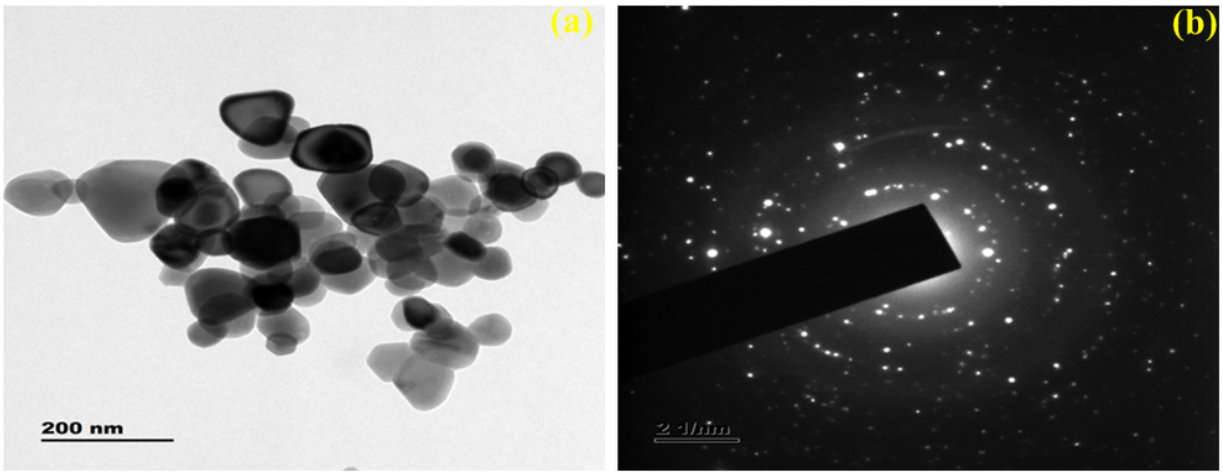

Figure 4

a) TEM images of Mg doped ZnO at concentration2%, b) SAED pattern of Mg doped ZnO.

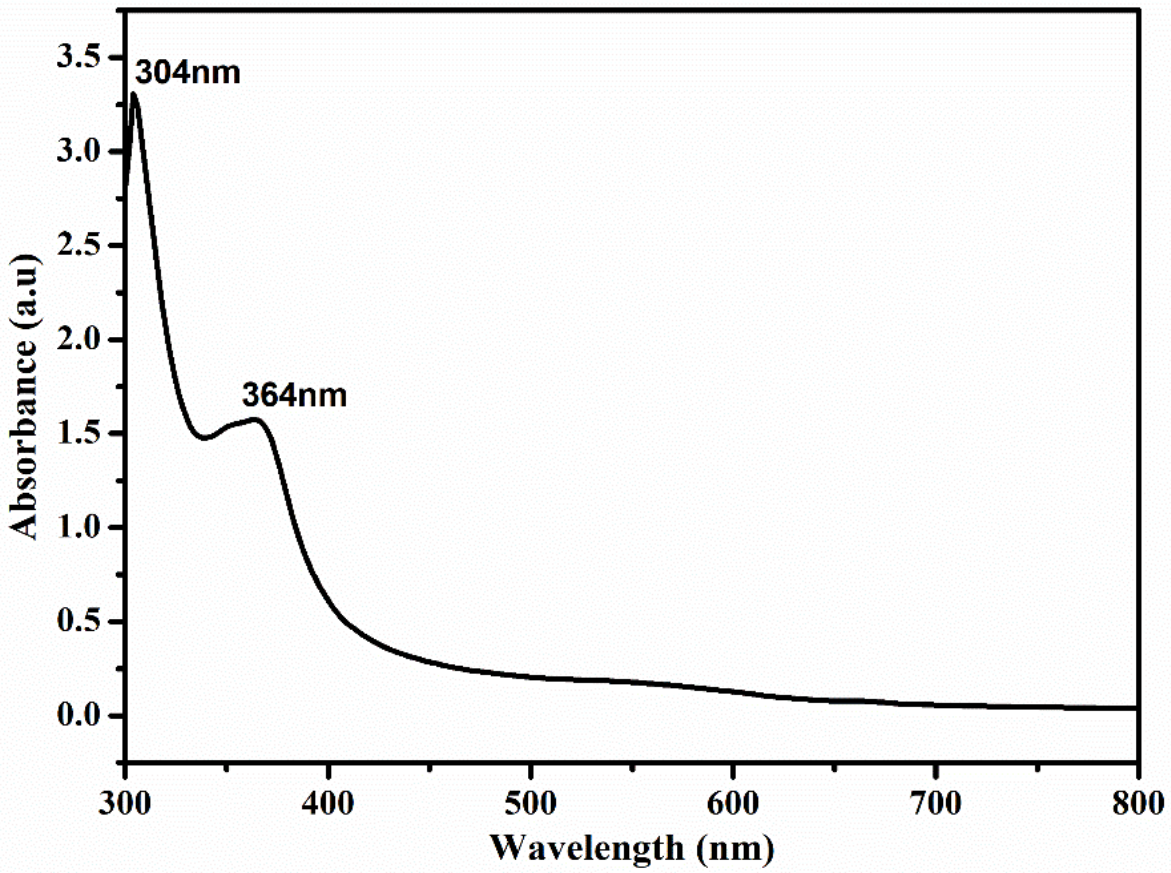

Figure 5

UV-Visible absorption spectra of terminalia cattappa leaves.

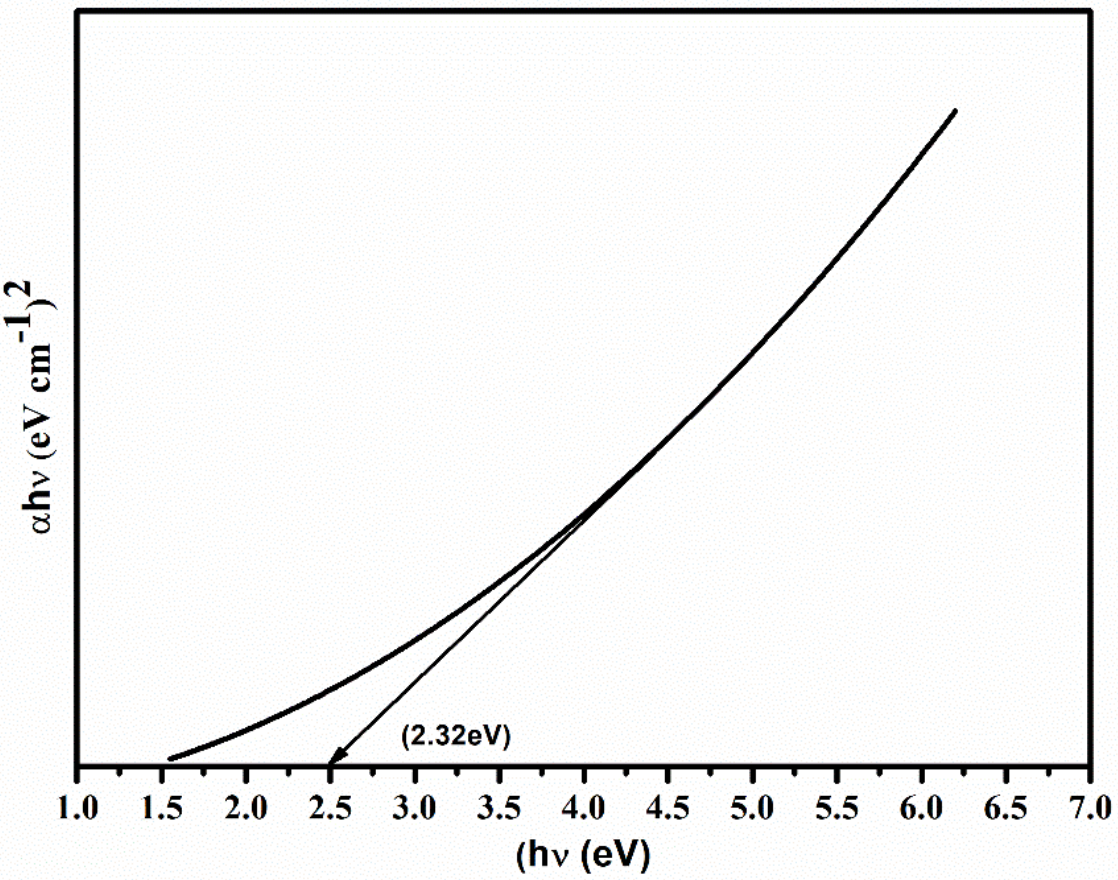

Figure 6

Band gap plot of Terminalia Cattappa leaves.

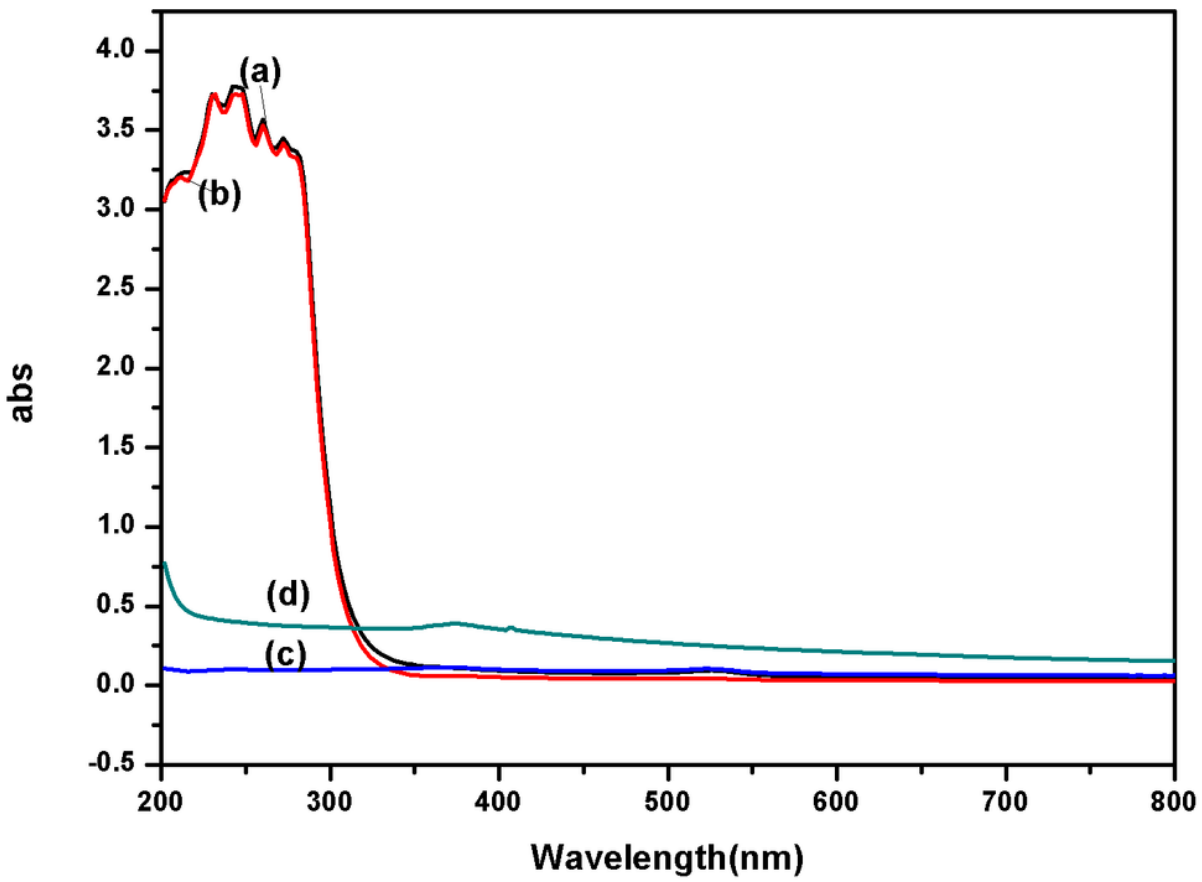

Figure 7

UV-Visible absorption spectra of Mg-Doped ZnO nanoparticles at various concentrations of a) 2%, b)4% ,c) 6% and d) 8%.

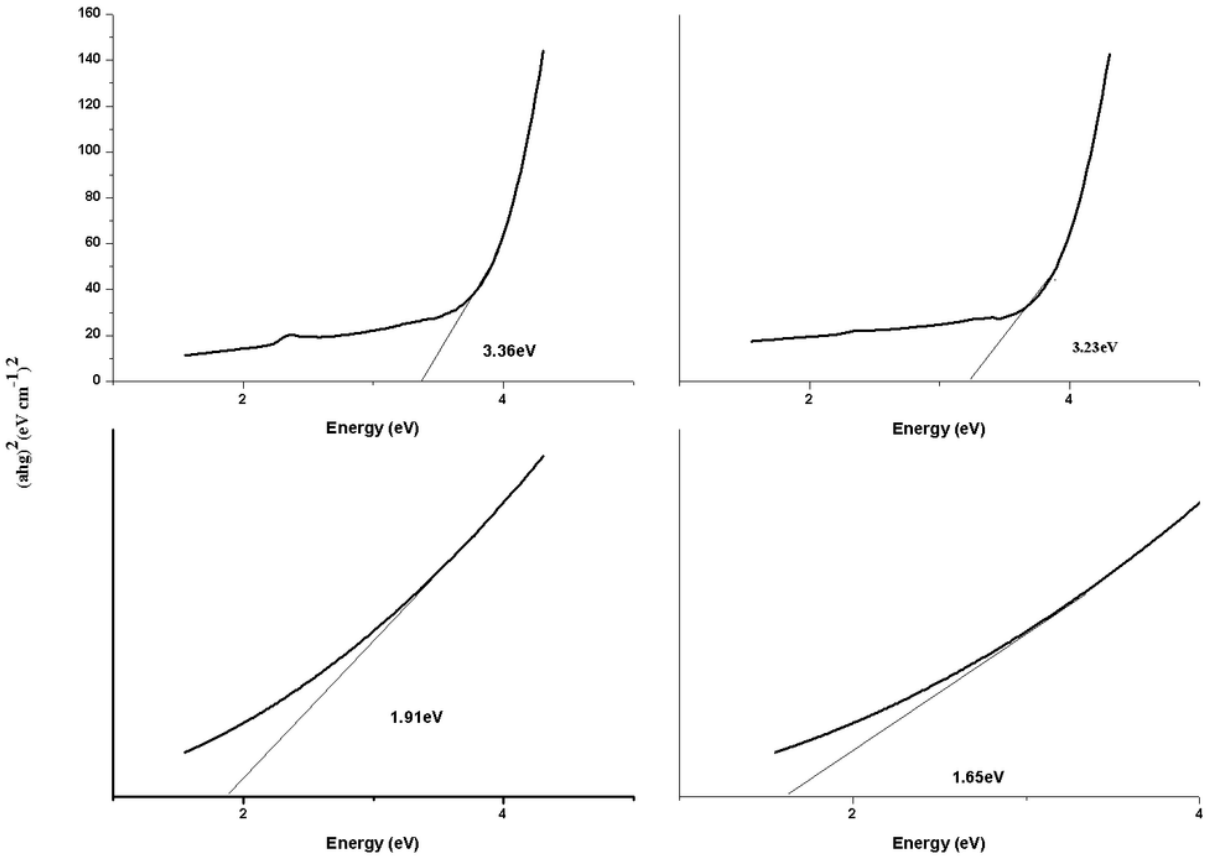

Figure 8

Bandgap values of Mg-doped ZnO nanoparticels at different concentration

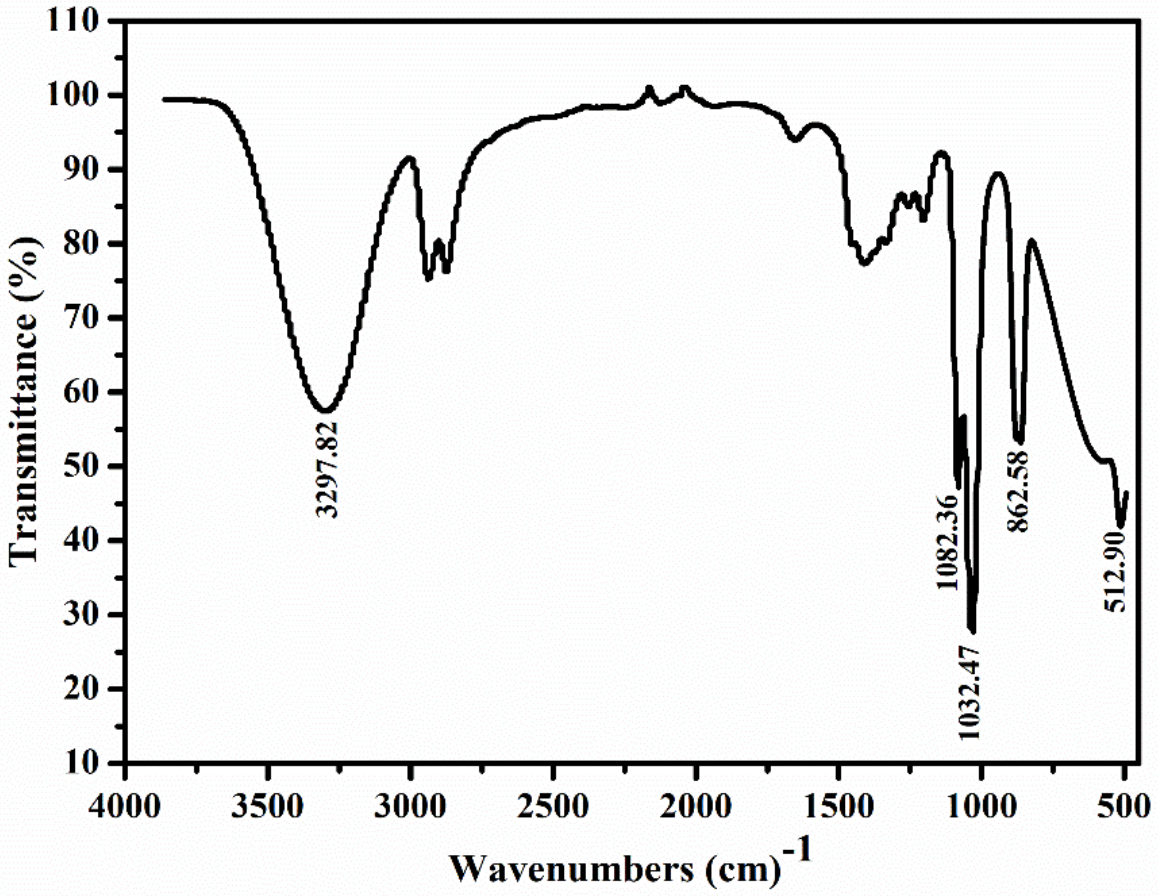

Figure 9

FTIR spectra of Terminalia Cattappa leaves

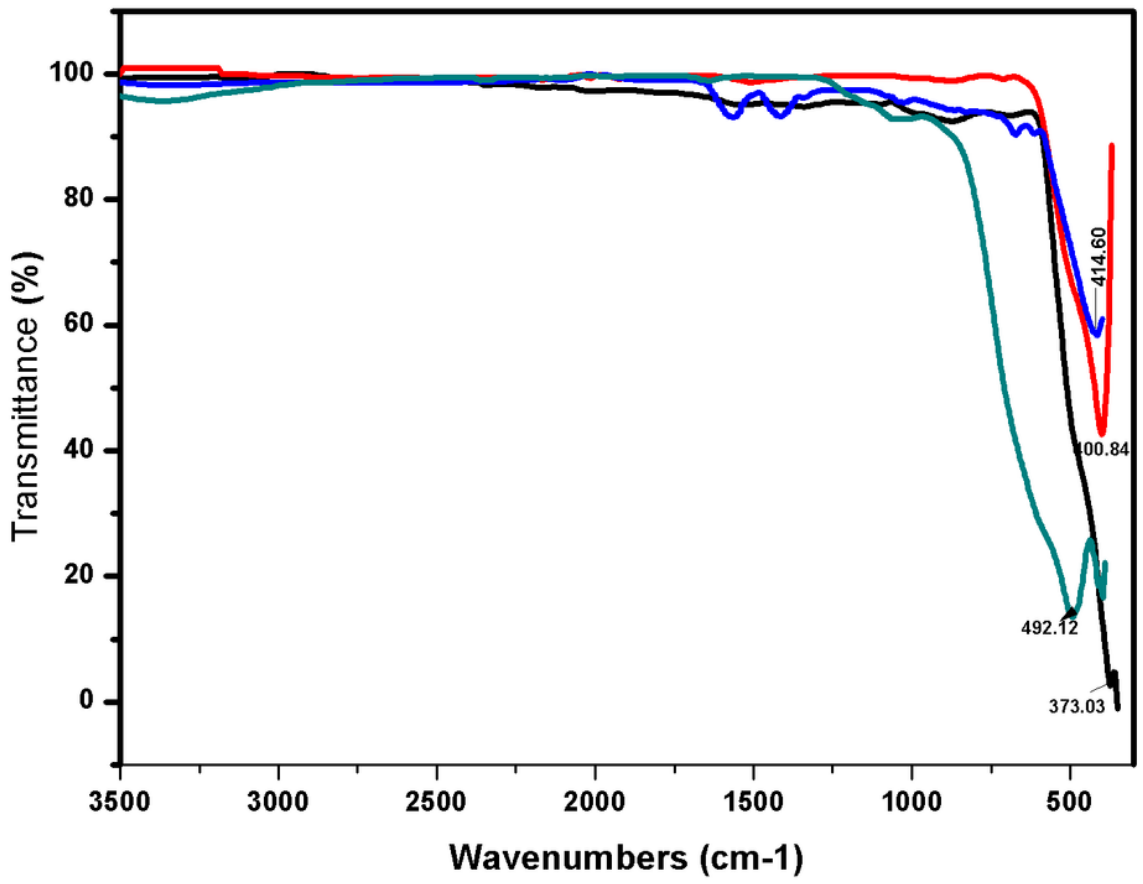

Figure 10

Transmittance spectra of Mg- doped ZnO nanoparticles at various concentrations of 2%,4%,6% and 8%.

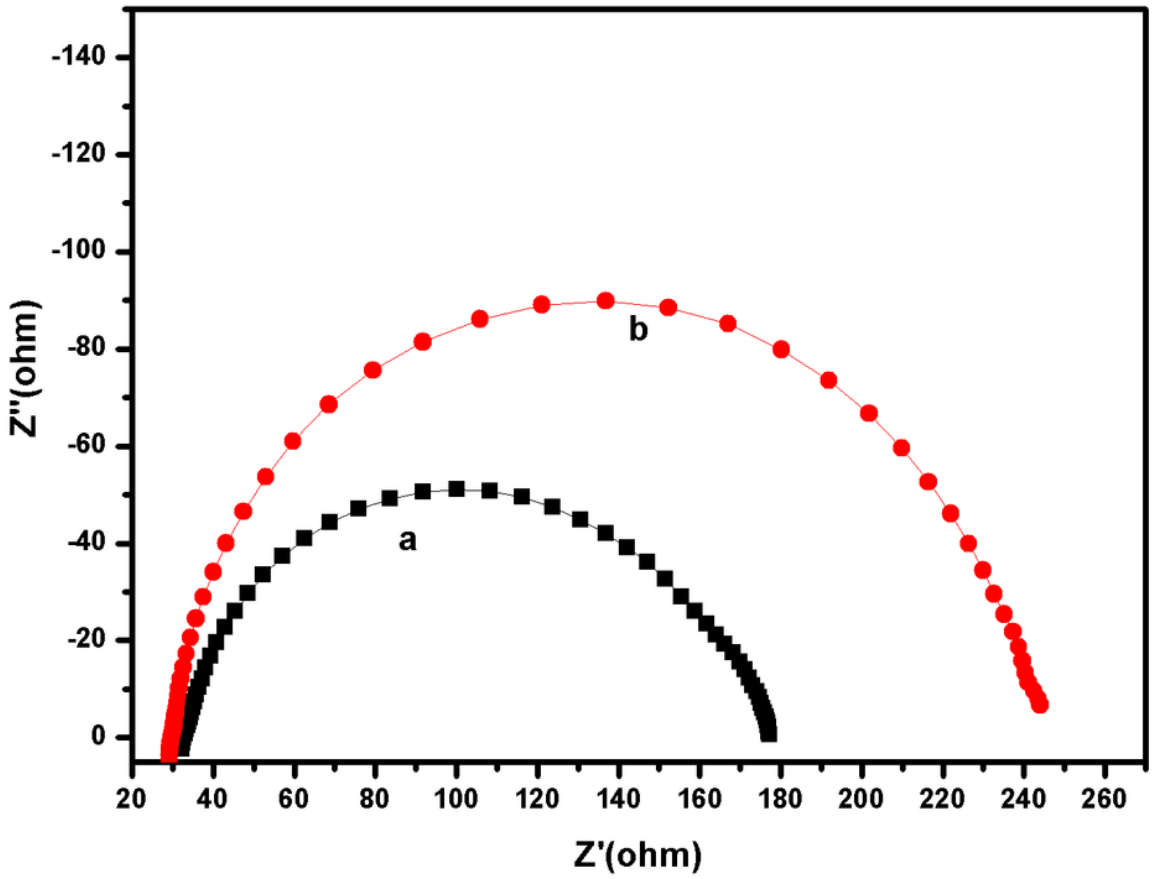

Figure 11

Nyquist plot of solar cell at Mg- doped ZnO of 2% and 8%

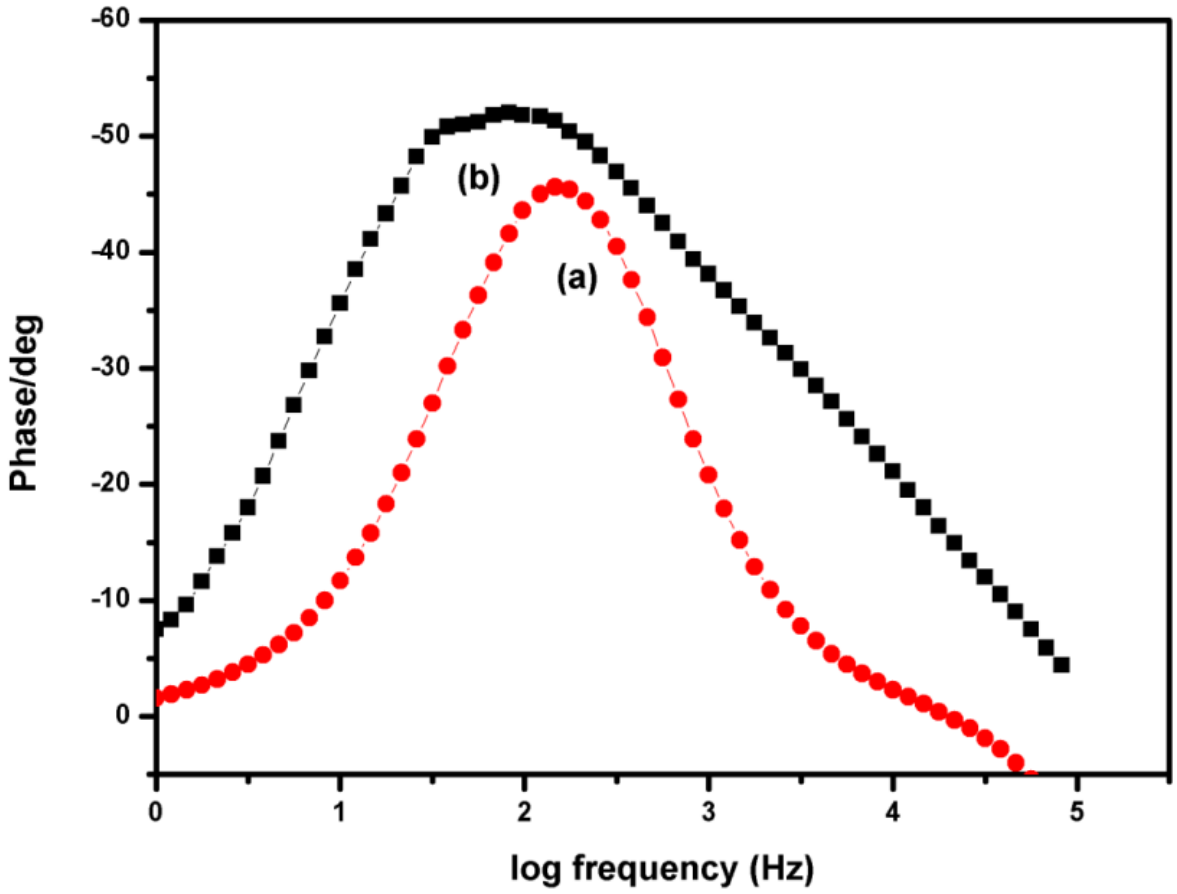

Figure 12

Bode plot of solar cells at concentration of 2% and 8%

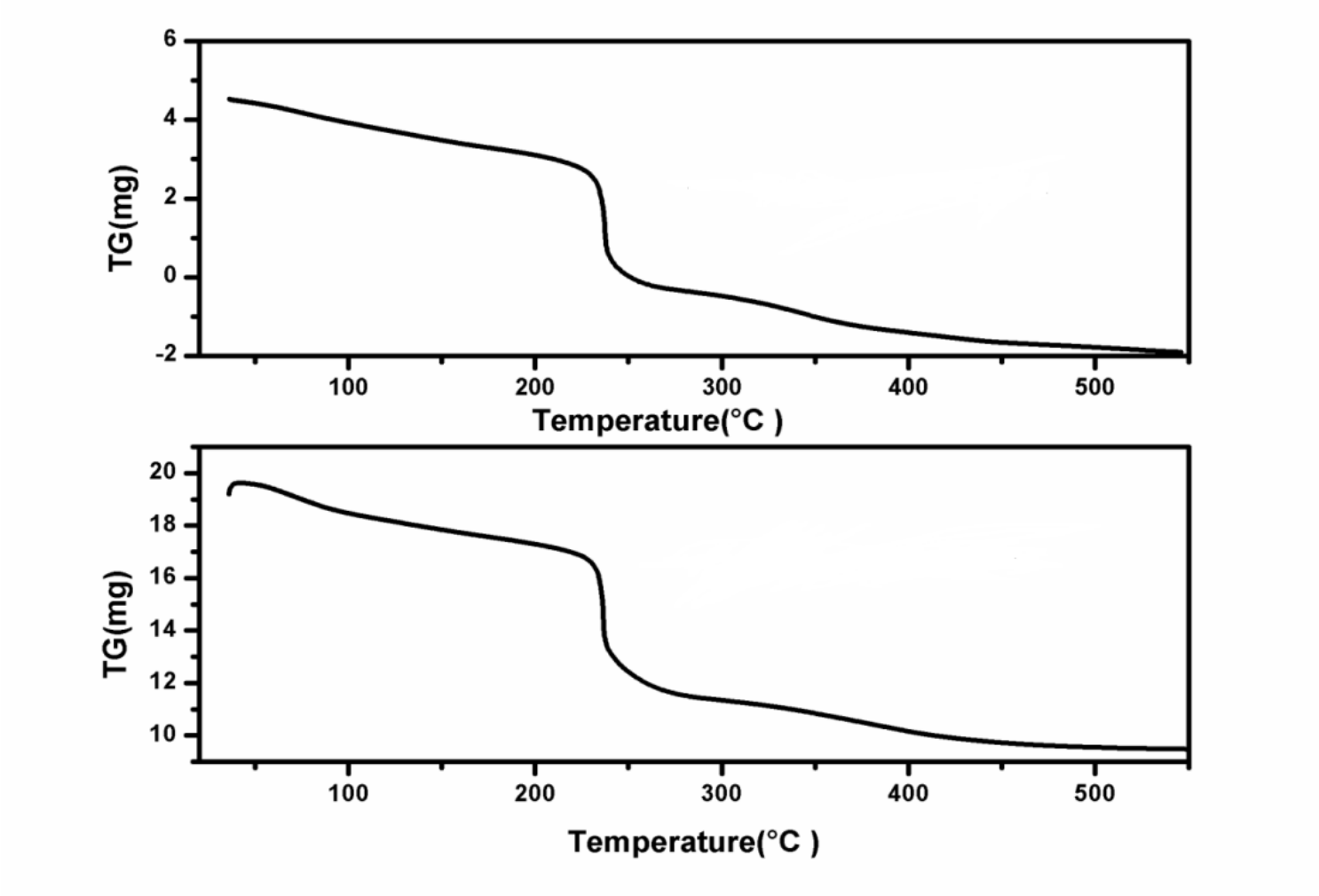

Figure 13

Thermogravimetric analysis of Mg doped ZnO at different concentration of 2% and8%

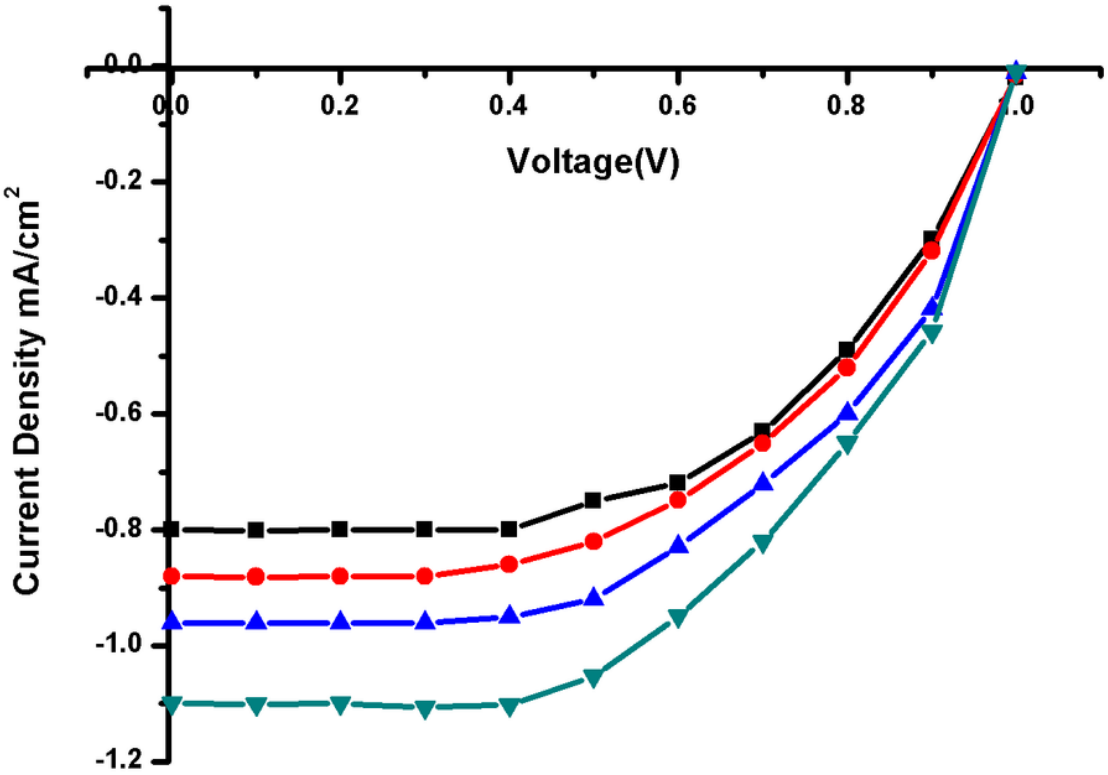

Figure 14

J-V curves for the DSSCs sensitized by terminalia cattappa. leaves extracts with Mg doped ZnO at 2%,4%,6% and 8%